

A Stochastic Model for Earthquake Rupture

Tsung-Hsi Wu (✉ tsung.hsi@g.ncu.edu.tw)

National Central University

Chien-Chih Chen

National Central University

Research Article

Keywords: earthquake rupture, friction process, stochastic dynamics, Langevin equation, Fokker–Planck equation

Posted Date: August 31st, 2023

DOI: <https://doi.org/10.21203/rs.3.rs-3301435/v1>

License:  This work is licensed under a Creative Commons Attribution 4.0 International License.

[Read Full License](#)

Additional Declarations: No competing interests reported.

A Stochastic Model for Earthquake Rupture

Tsung-Hsi Wu^{1*} and Chien-Chih Chen^{1,2}

¹*Department of Earth Sciences, National Central University, Zongda road, Taoyuan, 32001, , Taiwan.

²Earthquake-Disaster & Risk Evaluation and Management Center, National Central University, Zongda road, Taoyuan, 32001, , Taiwan.

*Corresponding author(s). E-mail(s): tsung.hsi@g.ncu.edu.tw;
Contributing authors: chienchih.chen@g.ncu.edu.tw;

Abstract

Analytical solutions for the dynamics of asymmetric many-body systems are impractical to obtain, and numerical solutions usually exhibit chaotic behavior if interactions between bodies are considered. To address these challenges, stochastic approaches have been widely employed in modelling many-body systems. Following Langevin's approach, we propose a stochastic dynamic model for the earthquake rupture process, in which complexity in degrees of freedom is reduced by introducing a random force that accounts for uncertainties in faulting plane heterogeneity and structural collisions. By treating the tectonic process as a Coulomb friction process, the proposed Langevin equation can be viewed as a stochastic variant of Newton's second law, thereby attributing physical significance to the equation through the realization of stochastic processes as sample paths. This study analyzes synthetic events generated numerically with the Langevin equation to determine the energy–duration relationship and solves the corresponding Fokker–Planck equation to obtain the theoretical rupture slip distribution. The results for the energy–duration relationship suggest the existence of a universal scaling law, with the scaling exponent varying under different slip velocity thresholds used to define synthetic events. Regarding the slip distribution, solutions obtained assuming relatively large external driving forces align closely with the truncated exponential model, characterizing rupture models of large earthquake events worldwide. The proposed Langevin equation establishes a physical foundation that elucidates the physics governing the scaling parameter of such laws and reveals the connection between the scaling parameter and the dissipative and environmental noise effects of the faulting system.

Keywords: earthquake rupture, friction process, stochastic dynamics, Langevin equation, Fokker–Planck equation

1 Introduction

2 Stick-slip frictional instabilities are fracture-like phenomena occurring on non-uniform
3 prestressed interfaces [1]; under this framework, earthquakes can be realized as stick-
4 slip events in a frictional process of a tectonic scale. The stick-slip explanation of
5 earthquakes can be dated back to Brace and Byerlee [2], who considered earthquakes
6 as transitory phenomena subject to long-term friction within the Earth's crust.

7 Friction, specifically Coulomb friction, arises from interactions between geometric
8 structures on contacting interfaces [3]. Haessig and Friedland [4] further conceptualized
9 Coulomb friction as a macroscopic phenomenon comprising successive and repetitive
10 stick-slip events. The notion of stick-slip is analogous in the context of Coulomb friction
11 and earthquakes, representing the physical bonding and bonding failure under
12 stressed conditions. In seismology, bonding refers to interlocking between surfaces,
13 while bonding failure corresponds to the breakdown of interlocked asperities. Due
14 to this similarity, laboratory experiments on Coulomb friction have been extensively
15 employed to study earthquake physics, as they exhibit stick-slips resembling earth-
16 quakes on a smaller scale [2, 5–11]. Similar to earthquakes, complex and chaotic
17 behavior is often observed in laboratory-scale Coulomb friction processes. To repre-
18 sent realistic contact conditions, stochastic process or fractal surface models had been
19 commonly applied in the simulation of friction processes [12, 13].

20 Despite the inherent inaccessibility of critical material or frictional strengths, slip
21 nucleation in earthquakes shares fundamental mechanisms with laboratory stick-slip
22 frictional processes. The complexity of earthquake phenomena is a critical key point
23 highlighted in seismology. Earthquake rupture is in general suggested occurring within
24 a spatially heterogeneous stress and strength environment [14], involving a combina-
25 tion of frictional slip instability and rock fracture [15]. Considering the scale and the
26 basically uncountable number of degrees of freedom, obtaining analytical molecular
27 dynamics solutions for the interactions between the physical bodies composing a fault-
28 ing system is impossible [16]. On the other hand, scaling laws, such as the relationship
29 between seismic moment and fault size, seismic moment and rupture duration, and
30 the distribution of earthquake magnitudes (Gutenberg-Richter law), have been exten-
31 sively validated [17–22]. These scaling laws suggest that earthquakes share similar
32 fundamental mechanisms regardless of their scale, and this scaling invariance is known
33 as the self-similar nature of earthquakes.

34 Self-similarity is a property related to fractality; in seismology, both concepts
35 involve the repetition of patterns at different scales that summarize the complexity of
36 the earthquake. A self-similar process is a type of stochastic process where the sta-
37 tistical properties based on measurements of different scales remain invariant. In the
38 context of earthquake rupture, consistent self-similarity are observed from laboratory
39 to field, and manifests in various faulting properties [23–29]. Empirical scaling laws
40 obtained from this kind of observations not only provide fundamental insights into
41 the nature of earthquake ruptures, but also serve as a basis for developing models and
42 conducting simulations. In many studies, slip/stress distributions, ground motion, and
43 fault surface geometries are assumed to be stochastic, aiming to create more realistic
44 rupture models and facilitate improved estimation or prediction [30–34]. Additionally,
45 high-frequency ground motions are very likely to be attributed more to the collision

46 of structures during the friction process rather than abrupt slips [34]. These indica-
47 tions collectively support the conclusion that the general earthquake rupture process
48 is a dissipative stochastic process.

49 The study of stochastic processes was initiated by Einstein in 1905, when he suc-
50 cessfully modeled the dynamics of Brownian particles using the kinetic theory of
51 heat [35, 36]. Einstein’s approach, known as the Fokker-Planck equation (FPE), pro-
52 vides the probability density function (PDF) of particle velocity. On the other hand,
53 Langevin, in 1908, introduced the Langevin equation to describe Brownian motion
54 [37]. By incorporating the effect of the random environment into a single noise term,
55 Langevin’s approach effectively reduces the number of degrees of freedom in the
56 equation of motion, making solving the problem feasible.

57 In our study, we state that the general earthquake rupture process is a stochastic
58 friction process with deterministic external and stochastic internal sources providing
59 the momentum for the rupture to propagate. Inspired by the Brownian motion, we
60 explore the capability of applying Langevin’s approach to obtain statistical properties
61 and theoretical scaling laws in seismology. The idea is simple: we consider the seis-
62 mogenic process at a tectonic timescale as a steady-state process of Coulomb friction
63 with random fluctuations, and we consider earthquake events to be transient stick-slip
64 events during the process. On the basis of the Langevin equation and its corresponding
65 FPE, we numerically generate stochastic friction processes and derive the theoretical
66 PDF for rupture slips. The results show that both the analytical solution of the FPE
67 and the numerical solutions of the Langevin equation coincide with the truncated
68 exponential (TEX) model proposed by Thingbaijam and Mai (2016). Furthermore,
69 numerical simulation of the Langevin equation suggests a universal energy-duration
70 scaling law, where the scaling exponent lies in the range of observed moment-duration
71 relationships. The proposed Langevin equation unveils the physics behind the scaling
72 parameter in scaling laws, connecting it to the average dissipative effect, environmen-
73 tal noise effect, and average driving force of a faulting system. By shedding light on the
74 underlying physical mechanisms of earthquakes, a deeper understanding of these scal-
75 ing laws can potentially contribute to future advancements in assessing the potential
76 for earthquake clustering or cascading events in a probabilistic manner.

77 **2 Stochastic dynamics for heterogeneous friction**

78 Both frictional slip and rock fracture are the process of degradation of shear strength,
79 with associated dissipation of energy through cracking, plastic deformation or com-
80 minution with ongoing slip. With considerable circumstantial evidences, Ohnaka et al.
81 [15] pointed out that earthquake rupture is a mixed process of frictional slip and
82 fracture of intact rock. Later in Ohnaka [39], a unified framework for comprehend-
83 ing earthquake, frictional slip, and fracture of rock is established based on laboratory
84 experiments and field observations of earthquakes. The very key role in the unified
85 constitutive law proposed by Ohnaka [39] is the “characteristic length”, which directly
86 associates with the fractal geometrical irregularities and the average size of breakdown
87 zones (also frequently denoted as “asperities” or “barriers”) of the faulting surfaces.
88 Breakdown zones refer to strong patches of high rupture resistance on a fault, at

which strain energy accumulates during interseismic period. The assumption of heterogeneous strong patches in a fault system sits in the center of the barrier model [e.g., 40–43] to explain the dynamics of earthquake as part of the stick-slip behavior in tectonic motion. Based on granite shearing experiments under high confining pressure, it has been suggested that generating a new fracture plane requires identical deformation energy as activating a preexisting fault [44, 45], and thus the activation of an earthquake is often put into analogy with the onset of sudden slip of a slider in a spring–slider system.

The simplest representative model treating an earthquake fault system as a many-body system is the spring–block model, with the model of Burridge and Knopoff (1967) being the first of its kind to involve massive blocks. In many studies, an asperity or local strong patch on the sliding surfaces is simplified as an individual strain–energy-storing unit, such as a slider attached by a tensioned spring [e.g., 46, 47] or a bending bristle [e.g., 4, 48–50]. The spring–slider model provides a conceptual framework that connects the Coulomb failure criterion and Griffith’s theory of fracture to friction and material failure. The Coulomb failure criterion, which relates shear stress to normal stress, provides a phenomenological description of frictional behavior [51]. For earthquake rupture, it states that failure occurs when the shear stress reaches a critical strength that depends on material properties and the stress states underground. In the spring–slider model, this critical shear stress corresponds to the point at which the applied force exceeds the frictional resistance, causing the slider to slip. Griffith’s theory of fracture, on the other hand, focuses on the energy balance at the rupture front or crack tip [52]. According to Griffith’s criterion, failure occurs when the available energy (strain or potential energy release minus heat dissipation) exceeds the energy required to create new cracks or surfaces. In the spring–slider model, the rupture front corresponds to the location of the sliding slider, and the energy balance at this front determines whether the slip will keep propagating or cease. If the available energy exceeds the threshold necessary for creating cracks that lead to the activation of adjacent spring–slider units, slip continues, analogous to fracture propagation; otherwise, slip ceases.

Theoretically, we can deterministically predict the evolution of any macroscopic dynamical system with classical mechanics, but for systems with many degrees of freedom, the differential equations become explicitly unsolvable [53]. With the existence of asymmetry in a spring–slider system, the dynamics of the blocks easily exhibits deterministic chaos, leading to the hypothesis that an earthquake can be treated as a stochastic process [16, 54, 55]. In the propagation of rupture within a many-body system such as an earthquake faulting system, the forces at each successive rupture point are practically indeterminate. Aiming for obtaining sufficient number of model-based simulations, we follow Langevin’s approach to reduce the number of degrees of freedom by introducing a random force, regarding earthquake rupture as a stochastic process. In Langevin’s description for Brownian motion, the motion of Brownian particles in a heat bath is assumed to be memoryless and nondifferentiable [37], and therefore, the total force on a Brownian particle can be subdivided into a deterministic (classical) part and a random (thermodynamic) part. Considering a seismogenic environment where spontaneous failures persistently occur, we categorize the forces

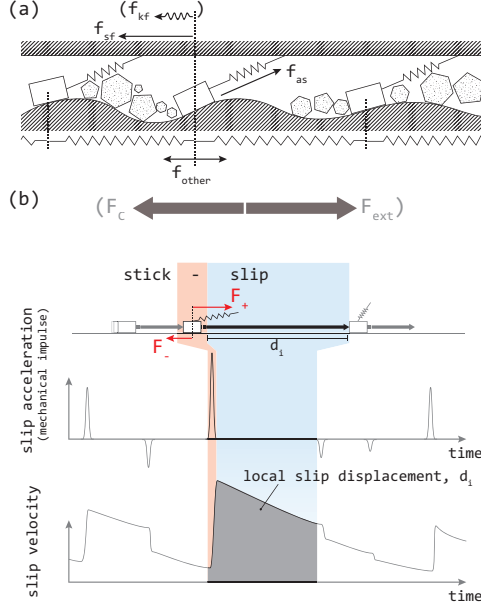


Fig. 1 Illustration of our idea of modeling the earthquake source process with the Langevin equation. (a) the illustration of the components of the system. (b) the time-force diagram with one stick-slip step emphasized with color. The resultant force that do positive work is denoted as F_+ , and that do negative works is denoted as F_- (with the + and - sign indicating the direction of energy transfer). The mechanical impulse in (b) is the sum of F_+ and F_- .

governing the dynamics into three terms: external deterministic, internal stochastic, and dissipative. The external driving force is required for the system to reach critical strain and stress conditions; it acts as the tectonic driving force. The internal stochastic force encompasses all internal interactions, including frictional and fracture failures arising from heterogeneous prestressed conditions, as well as collisions between structures. Finally, the presence of a damping term is necessary to dissipate kinetic energy and ensure physical reasonability.

To illustrate the proposed stochastic process for earthquake rupture, we start with a conventional spring-block model, as shown in Fig. 1 (a). This conceptual model consists of spring–slider pairs lying against the landscape, with arbitrarily scattered obstacles between sliders. In the diagram, obstacles represented by hexagons symbolize a broad sense of energy “sinks” that have to be filled, such as cracking energy, before rupture can progress further. The landscape interacts with sliders through friction, with the varying curvature of the landscape visualizing energy barriers that have to be overcome for rupture to occur. On the other hand, springs serve as units for storing strain energy and mediate interactions between masses. Arrows in the figure further depict forces balanced on a representative block, including kinetic friction (f_{kf}), static friction (f_{sf}), spring force (f_{as}), and interactions between blocks (f_{other}). These forces can be summarized as an equivalent dissipative force (F_C) and a driving force (F_{ext}), as displayed in Fig. 1 (b), where F_C and F_{ext} act in opposite directions due to their nature.

155 The net effect of forces balanced on the representative slider at rupture front influ-
 156 ences the speed of the rupture and controls its progression; however, it is practically
 157 unpredictable, as addressed before. Following Langevin’s approach, energy dissipation
 158 and momentum transfer in the rupture process are treated separately, with a random
 159 force accounting for the unpredictable variation in the momentum of the rupture front.
 160 As displayed in Fig. 1 (b), the stochastic process for earthquake rupture we are going
 161 to propose is depicted as a sequence of stick–dissipate–collide events occurring in suc-
 162 cession, where each event consists of an abrupt change in slip velocity of a random
 163 value and a dissipative phase.

164 Assuming a simple Coulomb dissipative force, a memoryless random force, and
 165 a constant external driving force, the Langevin equation for the stochastic rupture
 166 process is formulated as follows:

$$F_k(t) = \frac{dv(t)}{dt} = -F_C \frac{v(t)}{|v(t)|} + \Gamma(t) + F_{\text{ext}}. \quad (1)$$

167 In this equation, $F_k(t)$ represents the force acting on the system at time t , $\frac{dv(t)}{dt}$ is the
 168 derivative of the slip velocity with respect to time, F_C is the dissipative force, $v(t)$ is
 169 the slip velocity, $\Gamma(t)$ is the memoryless random force, and F_{ext} is the external driving
 170 force. Noted that the mass is omitted; the forces in eq. 1 are all in the sense of “per
 171 unit mass”.

172 Eq. 1 mathematically construct our conceptual model for earthquake rupture,
 173 describing rupture propagation as a step-by-step diffusion–dissipation process. The
 174 random force, $\Gamma(t)$, is alternatively called the “diffusional force” since it is the cause
 175 that makes the random variable to disperse over time (and the process is thus described
 176 to be “diffusive”); its mathematical definition is described in Sec. 3. Without the ran-
 177 dom force, Eq. 1 describes only the macroscopic behavior of a Coulomb frictional
 178 process; that is, a steady rupture just like a block smoothly sliding on table.

179 3 Particular solutions from the Langevin equation 180 of Coulomb friction and the analytic solution 181 from the Fokker–Planck equation

182 The total force in a Langevin equation is always constituted by two terms: the drift
 183 term for deterministic forces and the diffusional term for thermodynamic/random
 184 forces. In Eq. 1, the drift term is composed of the damping of Coulomb friction
 185 ($-F_C \frac{v(t)}{|v(t)|}$) and the external force (F_{ext}); the diffusional term is the random force
 186 ($\Gamma(t)$). The diffusion term $\Gamma(t)$ in Eq. 1 is a time-independent random fluctuating force
 187 responsible for chaotic interactions and collisions and is defined by the time derivative
 188 of the Wiener process $W(t)$ to enable analytical calculation. By reducing the number of
 189 degrees of freedom in the many-body system to only one, the motion of an entity (or a
 190 body) in the system can be represented by the motion of the representative Brownian
 191 particle. The relation between $\Gamma(t)$ and the standard Wiener process ($W(t)$) is:

$$\Gamma(t) \equiv \sqrt{2D} dW(t)/dt, \quad (2)$$

192 satisfying [56, 57]:

$$\langle \Gamma(t)\Gamma(s) \rangle = 2D\delta(t-s), \quad (3)$$

193 where the diffusion coefficient D reflects the average strength of the random fluctuation
 194 $\Gamma(t)$. By substituting the random force with the standard Wiener process in Eq. 2,
 195 we have the following equivalent stochastic differential equation (SDE) for Eq. 1, with
 196 $v(t)$ being the random variable for the (particle) slip velocity:

$$dv(t) = -F_C \frac{v(t)}{|v(t)|} dt + F_{\text{ext}} dt + \sqrt{2D} dW(t). \quad (4)$$

197 In Eq. 4, $dW(t)$ is also a random variable comprising independent and equally proba-
 198 ble Gaussian-distributed steps with standard deviation $\pm\sqrt{dt}$. Accordingly, a stepwise
 199 sample path $v_p(t) = \{V_0, V_1, V_2, \dots, V_k, \dots, V_N\}$ can be constructed by subdividing a
 200 given time interval $[0, T]$ into N subintervals, $0 = t_0 < t_1 < t_2 < \dots < t_k < \dots < t_N =$
 201 T , with $V_{k+1} - V_k$ being $(-(F_C V_k / |V_k|) + F_{\text{ext}})(t_{k+1} - t_k) + \sqrt{2D} dW(t_k)$ [58]. The
 202 Langevin equation is essentially an SDE where the realizations of the random variable
 203 (i.e., the particular solutions or sample paths) have little meaning until the statistics
 204 are computed. Similar to the deterministic equation of motion (Newton's second law),
 205 the Langevin equation has a straightforward physical meaning; however, it cannot
 206 predict the exact trajectory of a Brownian particle. Instead, the Langevin equation
 207 is usually used to obtain a large number of particular solutions for an ensemble
 208 prediction.

209 The Langevin equation always gives statistically equivalent results as its corre-
 210 sponding FPE, which was demonstrated later [59, 60]. In contrast to the Langevin
 211 equation, the FPE is a partial differential equation that describes the evolution of
 212 the probability distribution of a fluctuating macroscopic variable, for example, y . By
 213 solving the FPE, the stochastic process is realized as the evolution of the probability
 214 distribution of y , denoted $P(y, t)$. The well-known diffusion equation describing the
 215 collective behavior of an assembly of free Brownian particles is a simple example of the
 216 FPE [59, 61]. The FPE and the Langevin equation are mathematically equivalent [59],
 217 but they describe Markovian random walks from two entirely different perspectives.
 218 In practice, only a few FPEs can be solved analytically, whereas obtaining the PDF
 219 according to particular solutions of the Langevin equation is computationally time-
 220 consuming [62]. For the Langevin equation in the form of $dy(t)/dt = A(t, y(t)) + \Gamma(t)$,
 221 the corresponding FPE is [59]

$$\frac{\partial P(y, t)}{\partial t} = -\frac{\partial}{\partial y} \left(A(t, y(t))P(y, t) \right) + D \frac{\partial^2}{\partial y^2} P(y, t) \quad (5)$$

²²² By substituting the drift term $A(t, y(t))$ with $-F_C v(t)/|v(t)| + F_{\text{ext}}$, we can obtain the
²²³ FPE for the stochastic process of Coulomb friction

$$\frac{\partial P(v, t)}{\partial t} = -\frac{\partial}{\partial v} \left(\left(-F_C \frac{v(t)}{|v(t)|} + F_{\text{ext}} \right) P(v, t) \right) + D \frac{\partial^2}{\partial v^2} P(v, t). \quad (6)$$

²²⁴ Assuming steady-state conditions, where the system is far from the initial condition
²²⁵ and the process is stationary, meaning that the PDF is invariant with time
²²⁶ ($\partial P(v, t)/\partial t = 0$), we have:

$$\left(-F_C \frac{v}{|v|} + F_{\text{ext}} \right) P_{\text{st}}(v) = D \frac{\partial}{\partial v} P_{\text{st}}(v). \quad (7)$$

²²⁷ Hence, the steady-state solution is given by:

$$P_{\text{st}}(v) = P_0 \exp \left(\frac{F_{\text{ext}} v}{D} \right) \exp \left(\frac{-F_C v |v|}{D} \right), \quad (8)$$

²²⁸ or simply

$$P_{\text{st}}(v) = \begin{cases} P_0 \exp \left(\frac{F_{\text{ext}} + F_C}{D} v \right), & \text{for } v \leq 0 \\ P_0 \exp \left(\frac{F_{\text{ext}} - F_C}{D} v \right), & \text{for } v > 0 \end{cases} \quad (9)$$

²²⁹ 4 Results

²³⁰ 4.1 The empirical distribution of rupture slips

²³¹ Eq. 9 theoretically shows that the distribution of slip velocities during a steady-
²³² state friction process is a double-sided exponential function. As an example, Fig. 2
²³³ demonstrates comparisons between the analytically obtained steady-state solutions
²³⁴ $P_{\text{st}}(v)$ of the FPE (Eq. 8 or Eq. 9), shown as the red curves, and the ensemble-
²³⁵ predicted distributions as histograms, with $D = 10$, $F_C = 1$, and $F_{\text{ext}} = 0.9$.
²³⁶ Each histogram subplot comprises values sampled from 10^4 sample paths of $v(t)$ at
²³⁷ $t = 713, 1571, 2428, 3285, 4143$, and 5000 , with each sample path being obtained
²³⁸ by numerically solving the Langevin equation (Eq. 1 or Eq. 4). The red curves in the
²³⁹ figure are the theoretical probability distributions of v at $t \rightarrow \infty$; as a matter of course,
²⁴⁰ the histograms of the ensemble-predicted values at larger t approximate the red curves
²⁴¹ better than those at smaller t . For real large earthquakes ($M_w \geq 5$), Thingbaijam and
²⁴² Mai demonstrated that the TEX distribution best characterizes the empirical distri-
²⁴³ bution of rupture slips in either an individual or an average sense, as demonstrated
²⁴⁴ in Fig. 3. The authors examined the goodness of fit rigorously over the TEX distribu-
²⁴⁵ tion in addition to other well-known distributions, including the exponential (EXP),
²⁴⁶ Weibull, Gamma, and lognormal distributions, by analyzing 190 source models of
²⁴⁷ events worldwide. They concluded that the TEX distribution generally exhibits the

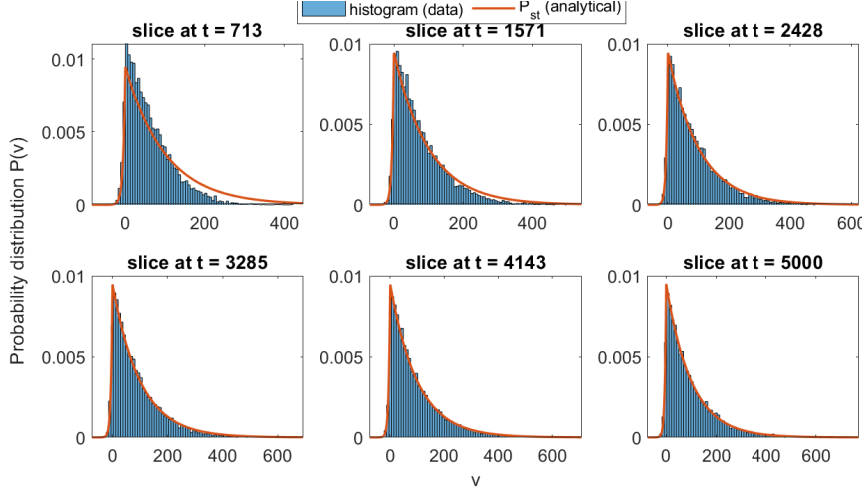


Fig. 2 The probability distribution of slip velocity calculated from an ensemble of samples sampled from total 10^4 realizations at different time (the histogram), and the steady-state solution $P_{st}(v)$ (see Eq.8 and 9) (the red curve), in which $D = 10$, $F_C = 1$, $F_{ext} = 0.9$.

best fit to the slips along fault planes, especially at larger slip values. In their study, the fitting function was expressed in the form of the complementary cumulative distribution function (CCDF) to avoid arbitrarily choosing the data bin size and to better distinguish the fitting results at large slips. In addition, the CCDF for a non-truncated EXP distribution function $f_{EXP}(v) = (1/v_c) \exp(-v/v_c)$ is also an EXP distribution:

$$1 - F_{EXP}(v) = \exp\left(-\frac{v}{v_c}\right), \quad (10)$$

where $F_{EXP}(v) = 1 - \exp(-v/v_c)$ is the cumulative distribution function (CDF) of $f_{EXP}(v)$. For the TEX distribution $f_{TEX}(v) \equiv f_{EXP}(v)/F_{EXP}(v_{max})$, its CCDF form is

$$1 - F_{TEX}(v) = \frac{\exp(-v/v_c) - \exp(-v_{max}/v_c)}{1 - \exp(-v_{max}/v_c)}, \quad (11)$$

where $F_{TEX}(v)$ is the CDF of $f_{TEX}(v)$. The TEX distribution function is a conditional distribution obtained by restricting the domain of the original function. When calculating the distribution of either a simulated or an empirically observed physical quantity, the largest value in the dataset must be finite. Thus, empirically calculated statistics can more often fit the TEX distribution better than the original form can. To demonstrate how local slips $((t_{k+1} - t_k)V_k \text{ or } v_p(t)dt)$ in an individual realization of the Langevin friction process fit the TEX and EXP functions, we generate three sample paths of different durations with the parameters $D = 5$, $F_C = 1$, and $F_{ext} = 0.9$. Relatively large values of D and F_{ext} (relative to F_C) are chosen because they generally produce larger slips and might better meet the physical conditions for large earthquakes. Following the method of Thingbaijam and Mai, we calculate the CCDF

of slip velocities for an individual realization or set of realizations and fit their CCDF with the CCDFs of the EXP (Eq. 10) and TEX (Eq. 11) distribution functions. The fitting results are demonstrated in Fig. 4. The scale parameters (v_c) are estimated by nonlinear least-squares fitting of the TEX or EXP model to the empirical CDF. In Fig. 4 (a), (b), and (c), the empirical CDF is the slip velocity distribution with uniform temporal sampling from one realization of the stochastic process, and the durations are 100, 1000, and 10000 simulation times (s.t.), respectively. In Fig. 4 (c), (d), and (f), the empirical CDF is calculated in the same way but from 1000 realizations for each duration to ensure that the result is robust. Note that we take the modulus of the signed velocities before calculating the CDF; that is, the absolute values of the negative velocities are added to the population of positive values. The results confirm that for sample paths of either short or long duration, the distribution exhibits a TEX shape and generally fits a TEX distribution better than an EXP distribution (i.e., the TEX fitting exhibits a lower R-squared (R^2) value or mean squared error (MSE)). Eq. 9 demonstrates the theoretical probability distribution (P_{st}) for the slip velocity of a steady-state Coulomb friction process. Using integration by parts, we can obtain the expectation $\langle v \rangle$ by treating positive and negative velocities separately:

$$\langle v \rangle = \int_{-\infty}^{\infty} v P_{st}(v) dv = -\frac{2DF_{ext}}{F_{ext}^2 - F_C^2}, \quad (12)$$

where

$$\langle v^- \rangle = \int_{-\infty}^0 v P_{st}(v) dv = -\frac{D}{2F_C} \frac{F_C - F_{ext}}{F_{ext} + F_C} \quad (13)$$

and

$$\langle v^+ \rangle = \int_0^{\infty} v P_{st}(v) dv = -\frac{D}{2F_C} \frac{F_C + F_{ext}}{F_{ext} - F_C}, \quad (14)$$

with F_{ext} assumed to be positive. As demonstrated by Eq. 12, F_{ext} critically contributes to the expected velocity ($\langle v \rangle$), especially when $F_{ext} \rightarrow F_C$. For example, in the case of $F_{ext} = 0.9F_C$, $|\langle v \rangle|$ is nearly 47 times greater than that in the case of $F_{ext} = 0.1F_C$ given the same D . Furthermore, in the case of $F_{ext} = 0.9F_C$ with $F_{ext} > 0$, positive velocities are overwhelmingly dominant in the population, as we have $|\langle v^+ \rangle| / |\langle v^- \rangle| = 361$. In this case, owing to the decay exponent for $v < 0$ (i.e., $1.9F_C/D$) being much larger than that for $v > 0$ (i.e., $0.1F_C/D$), according to Eq. 9, the probability density decays very quickly, as exemplified in Fig. 2. The EXP model and its truncated form, the TEX distribution, were established based on large events, while the physical condition reflected by large F_{ext}/F_C is particularly favorable for generating large events in our simulation. Thus, the relationships between the scale parameter (u_c in Fig. 3 or v_c in Fig. 4) and the physical parameters in the Langevin equation (F_{ext} , F_C and D) can be established, as the FPE solution generally approximates a single-sided exponential function for large F_{ext}/F_C according to Eq. 9. The single-sided exponential function (e.g., $P_0 \exp\left(\frac{F_{ext}-F_C}{D}v\right)$ for $F_{ext} > 0$) can be rewritten as the EXP model $P_0 \exp(-v/v_c)$. Hence, the relationship $v_c \equiv -\frac{D}{F_{ext}-F_C}$ is established, providing the physical basis for the empirical TEX model for earthquake rupture slips.

Table 1 The nonlinear fit to energy dissipated ($E_{\text{diss}} = F_C d$) and durations T of events with $\log T = c_1 + c_2 \log E_{\text{diss}}$. Events are defined by threshold $thr = 0$ from particular solutions generated with different diffusion coefficient (D), Coulomb friction parameter (F_C), and external force (F_{ext}) denoted in each row.

D	F_C	F_{ext}	$\langle v \rangle$	c_1	c_2
0.1	0.1	0.01	0.20	2.39	0.65
0.1	0.1	0.05	1.33	2.58	0.57
0.1	0.1	0.09	9.47	2.18	0.72
0.1	10	1	0.00	-2.04	0.41
0.1	10	5	0.01	-1.07	0.57
0.1	10	9	0.09	-0.67	0.65
0.1	1	0.1	0.02	0.73	0.62
0.1	1	0.5	0.13	0.83	0.64
0.1	1	0.9	0.95	0.91	0.66
1	0.1	0.01	2.02	1.70	0.65
1	0.1	0.05	13.33	1.63	0.66
1	0.1	0.09	94.74	2.16	0.61
1	10	1	0.02	-1.51	0.61
1	10	5	0.13	-1.44	0.64
1	10	9	0.95	-1.34	0.64
1	1	0.1	0.20	0.08	0.66
1	1	0.5	1.33	0.10	0.66
1	1	0.9	9.47	0.13	0.65
10	0.1	0.01	20.20	0.67	0.69
10	0.1	0.05	133.33	0.59	0.69
10	0.1	0.09	947.37	-0.17	0.75
10	10	1	0.20	-2.11	0.61
10	10	5	1.33	-2.12	0.63
10	10	9	9.47	-2.13	0.65
10	1	0.1	2.02	-0.56	0.64
10	1	0.5	13.33	-1.31	0.75
10	1	0.9	94.74	-0.84	0.68

4.2 The energy–duration scaling of the simulated events

The total energy released in an earthquake is the work done by the mean absolute shear stress ($\bar{\sigma}$) over the average slip distance (\bar{d}); it has the following relationship with the seismic moment [63]:

$$E = \bar{\sigma} S \bar{d} = \frac{\bar{\sigma}}{\mu} M_0. \quad (15)$$

Since practically quantifying the absolute shear stress is impossible, the total energy released in an earthquake event can be obtained only indirectly via a certain empirical relation; mostly, it is estimated as a portion of the seismic moment (M_0). Seismic moment has the dimensions of torque, being an equivalent representation of earthquake sources as a double-couple; it is defined as $M_0 = \mu S \bar{d}$ where μ is the rigidity, S the area of the fault, and \bar{d} the mean slip displacement [64]. Following the idea that an earthquake is decomposable, the equivalent double-couple of an event is thus a

314 composition of a collection of smaller double-couples, with each resulting in a stick-
 315 slip event. Now go back to Eq. 1, in the friction process of one-dimensional Brownian
 316 motion the concept of “area” does not exist, and the total amount of energy released
 317 in stick-slip eventually equals the energy dissipated in the friction process. Thus, we
 318 let the term $-F_C v/|v|$ in Eq. 1 to play the role of the term $\bar{\sigma}S$ in Eq. 15 that we
 319 can have discussions on the issue of energy–duration relation. The energy dissipated
 320 (E_{diss}) in a realization ($v_p(t)$) of the stochastic process can be calculated simply by

$$E_{\text{diss}} = \int_{x=0}^d F_C dx = \int_{t=0}^T F_C v_p(t) dt. \quad (16)$$

321 Then, assuming a constant Coulomb friction, the total amount of energy dissipated
 322 by the representative Brownian particle is $E_{\text{diss}} = F_C d$, where d is the accumulated
 323 slip during the process, as follows:

$$E_{\text{diss}} \propto d = \int_{t=0}^T v_p(t) dt \quad (17)$$

324 For a physically reasonable system, the absolute value of the driving force (F_{ext}) should
 325 lie within $\pm F_C$; otherwise, the diffusion process eventually diverges. When simulating
 326 the friction process of a tectonic plate, $F_{\text{ext}} = 0$ represents the condition under no
 327 tectonic stress, and local slips equally favor any direction; in contrast, if $F_{\text{ext}} = \pm F_C$,
 328 the process is close to diverging (i.e., $v \rightarrow \pm\infty$ as $t \rightarrow \infty$). Fig. 5 (a) demonstrates
 329 an example of a sample path, which is a realization of the slip velocity history as a
 330 particular solution of the Langevin equation (Eq. 4) with $F_C = 1$, $F_{\text{ext}} = 0.9$, and
 331 $D = 10$. By regarding an earthquake event (or a series of events) as a realization of the
 332 stochastic process governed by the Langevin equation, we define a simulated event as a
 333 segment of the particular solution divided by a certain threshold. That is, a simulated
 334 event starts when the slip velocity (v) of the representative Brownian particle exceeds
 335 a certain threshold and ends when v falls below that same threshold. The subdivision
 336 of an event is illustrated in Fig. 5 (b) and (c). The shaded areas in (b) and (c) indicate
 337 the intervals in which the sampled velocities all fall below the threshold $v_{\text{thr}} = 10$
 338 and are thus regarded as “undetectable” activities; in contrast, the intervals with an
 339 unshaded background (where $v > v_{\text{thr}}$) are hence regarded as the durations of the
 340 simulated events. To replicate the scenario of a tectonic process in which local slips
 341 are expected to favor a certain direction, we choose F_{ext} values of $+0.1F_C$, $+0.5F_C$,
 342 and $+0.9F_C$ against the diffusion coefficient $D = \{0.1, 1, 10\}$, and friction parameter
 343 $F_C = \{0.1, 1, 10\}$. We then generate a set of particular solutions of duration $\approx 10^6$
 344 s.t. with a step size of $dt = 10^{-3}$ (s.t.); that is, we establish a set of sample paths,
 345 with each path having $\sim 10^9$ steps. The numerical solutions are calculated according
 346 to Eq. 4 in an Eulerian scheme following the instruction manual of Cyganowski et al.
 347 (2001). By defining the lengths of the time series divided by the threshold $v_{\text{thr}} = 0$ as
 348 the durations (T) of the simulated events, we calculate the energy dissipated (E_{diss})
 349 in each event according to Eq. 16 to obtain the energy–duration relationship by fitting
 350 the data with

$$\log T = c_1 + c_2 \log E_{\text{diss}}. \quad (18)$$

351 The results are demonstrated in Table 1 and plotted in Fig. 6, showing that there is
 352 no obvious change in the exponent (c_2) of the scaling law (Eq. 18) over a wide range
 353 of physical conditions (parameter settings). The best-fitting c_2 is most commonly
 354 approximately 2/3; however, in a few cases, such as the sets of $\{D = 0.1, F_C =$
 355 $10, F_{\text{ext}} = 1\}$ and $\{D = 0.1, F_C = 10, F_{\text{ext}} = 5\}$, significant deviations of the best-
 356 fitting c_2 from 2/3 are observed. These deviations appear to be especially prominent
 357 when the population of a set is dominated by events with durations very close to
 358 the temporal resolution ($dt = 10^{-3}$) of the numerical simulation, that is, under the
 359 physical conditions that are favorable for generating very small events (e.g., high F_C
 360 and low D and F_{ext}). As observed in every $E_{\text{diss}} - T$ plot of Fig. 6 at approximately
 361 $T = 10^{-2}$ and below, the energies of the shortest events exhibit exceptionally broad
 362 scatter, largely because of the limitation imposed by the temporal resolution. In other
 363 words, the nonlinear fits can deviate considerably as a result of these widely scattered
 364 data when they compose the bulk of the population. Overall, it is clear that for all
 365 sets of physical conditions, the data points align well with the contour lines of $\log T =$
 366 $c_1 + (2/3) \log E_{\text{diss}}$, suggesting an invariant $E_{\text{diss}} - T$ scaling law.

367 5 Discussion

368 5.1 The energy–duration scaling

369 Basing on the Langevin equation, we study the energy–duration relationships of a set
 370 of simulated events under different physical conditions, with each subset having dif-
 371 ferent parameter settings of F_C , F_{ext} , and D . In each subset, the energies dissipated
 372 (E_{diss}) in the one-dimensional Langevin friction process scale with the event durations
 373 (T) with a nearly constant exponent of 2/3. The parameter settings vary widely, and
 374 thus, the average slip velocity expected for the events in each subset may span several
 375 orders of magnitude; however, the proportionality between E_{diss} and T in the log space
 376 barely changes, suggesting a universal scaling relationship between the energies dis-
 377 sipated and the event durations. Likewise, seismological observations tend to suggest
 378 a universal scaling relationship between the seismic moment and the event duration.
 379 Many studies have theoretically derived or empirically observed a scaling relation-
 380 ship of $T \propto M_0^{1/3}$ for regular (“fast”) earthquakes [63, 65–68]. In contrast, for slow
 381 earthquakes, a scaling law of $T \propto M_0$ has been observed worldwide for non-volcanic
 382 tremors, low- or very-low-frequency earthquakes, and slow slip events [69–71]. Due to
 383 the difference in the scaling exponent between these two scaling laws, the underlying
 384 dynamics were thought to be fundamentally different for fast and slow earthquakes
 385 [69, 72]. In a subsequent study conducted by Gomberg et al. [73], a transition in the
 386 scaling exponent of the power law was observed in both fast and slow slip populations.
 387 Relying solely on the dislocation theory [63, 74], the authors concluded that the tran-
 388 sition from $T \propto M_0^{1/3}$ to $T \propto M_0$ could originate from the geometric change in rupture
 389 growth from two dimensions to a single dimension: for bounded (one-dimensional)
 390 ruptures, their results suggest $T \propto M_0$ with the W-model assumption and $T \propto M_0^{1/2}$
 391 with the L-model assumption but suggest $T \propto M_0^{1/3}$ with either the W-model or
 392 the L-model assumption for unbounded (two-dimensional) ruptures. A more recent

study [68] further indicated that the $T \propto M_0$ scaling law for slow earthquakes could arise from the assembling of slow slip events under different physical conditions and reported that the scaling should be $T \propto M_0^{1/3}$ for a subset of slow slip events under the same physical conditions, implying that the underlying dynamics for slow and fast ruptures could be similar. Other studies have proposed or reported that the exponent n of the power law $T \propto M_0^n$ should lie between $1/3$ and 1 [72, 75–77], and the discrepancies in the moment–duration scaling law were attributed to the lower dimensionality of the model [77], different sensory thresholds [72], an artificially limited frequency range [75], or the criteria for defining an event [76]. Whether there exists a universal moment–duration scaling for either fast or slow earthquakes is still under debate. The almost invariant energy–duration scaling obtained in this study could shed light on the moment–duration scaling law for real earthquakes; however, many questions remain unanswered. First, the seismic moment is simply an attainable substitute for the energy released during the seismogenic process. In other words, for real earthquakes, the seismically or aseismically released energy can only be very roughly obtained through its relation to the seismic moment; for our model, to produce the physical “moment”, the relationships between the material rigidity and both the friction parameter and the diffusion coefficient in the governing equation must be established first. Second, we must develop a more complete understanding of the factors that may result in the transition of the scaling exponent but are otherwise unrelated to the underlying physical mechanism, for example, the dimensionality of the system or the criteria for defining an event. In this study, the proposed Langevin equation of friction is for a one-dimensional velocity space. Thus, the exponent in the scaling relationship may experience a transition if the equation is generalized for a space of two or more dimensions. In addition, the threshold for dividing the sample paths into simulated events is zero, which represents an unrealistic noise- and attenuation-free environment in which any activities with a slip velocity greater than zero are detectable. As the threshold changes, the exponent of the power law may change (displayed in the example of Fig. 7). Another issue is that the obtained energy–duration scaling, $T \propto E_{\text{diss}}^{2/3}$, is based solely on numerical simulations. Although this relationship is concluded according to simulations that cover several orders of magnitude of the friction and diffusion coefficient, much more cases remain untested. We may further narrow down the range of parameters according to the physical condition under which real-world earthquakes possibly occur and conduct a more complete analysis, if the link between the parameters in the Langevin equation to the real-world measurables is established. However, inductive reasoning by itself can never constitute a proof, no matter how many physical conditions have been tested; thus, analytical descriptions are required to explore this issue in greater depth.

5.2 Empirical slip distribution

For large F_{ext}/F_C ratios, we have theoretically demonstrated that the ensemble-averaged slip distribution should approximate an EXP distribution, and the time-averaged distribution of slips in sample paths of a certain finite length generally fits the TEX function better than it fits the EXP function. These results provide an alternative physical basis for the empirical TEX distribution of earthquake rupture slips and

indicate that the scale parameter (denoted v_c or u_c) in the TEX or EXP model can be directly linked to the underlying physical parameters (i.e. D , F_C , and F_{ext}) for generating the earthquake. The ensemble-averaged distribution is the distribution of data sampled at the same time point from a number of realizations of the random variable, while the time-averaged distribution is the distribution of data sampled from a single realization of the random variable as a time series. In summary, ensemble-averaged statistics are obtained as if we observe the physical quantity among a number of identical experiments, while time-averaged statistics are obtained by sampling the physical quantity in a single trial at a uniform temporal interval. The $P(v, t)$ in the FPE is an ensemble-averaged statistic and represents the probability density of having the value v at time t , whereas the empirical TEX law of Thingbaijam and Mai and the distribution of synthetic slip velocities demonstrated in Fig. 4 are time-averaged statistics since the data for calculating the distribution are sampled from one realization (or one earthquake). Generally, the ensemble-averaged statistics and the time-averaged statistics give disparate results since they are calculated in fundamentally different ways; in the cases where the ensemble-averaged statistics of samples at $t \rightarrow \infty$ always equal the time-averaged statistics of a sample path of infinite length, the stochastic process is said to be ergodic [61, 78–80]. Ergodicity of a dynamical system means that almost all possible states should have been visited and every state is recurrent in a sample path that is sufficiently long. Since the steady-state solution of the FPE (Eq. 6) is unique and its total integral converges, mathematically the proposed stochastic process of Coulomb friction (with $F_C > F_{\text{ext}}$) is ergodic according to the ergodic theorem [79, 80]. As a consequence of ergodicity, if a sample path is sufficiently long that the contribution due to different initial conditions to the time-averaged statistics is negligible, the average statistical properties of the dynamical system can be deduced from this single sample path. The ergodic nature of the stochastic process of Coulomb friction explains the fact that the time-averaged slip distributions also effectively fit the TEX or EXP model. Accordingly, we can better understand the results of the numerical simulations demonstrated in Fig. 4. For the sample paths of longer durations, the distribution of synthetic velocities generally fits either the EXP or the TEX model better, and the best-fitting parameter v_c better approximates the theoretical expectation calculated from the steady-state solution (47.5 for $D = 5$, $F_C = 1$, and $F_{\text{ext}} = 0.9$ according to Eq. 14). In summary, for a dynamical system that is not allowed to run for an adequately long time, even though the result may fit either the TEX or the EXP model well, the best-fitting parameter yields little to no useful information. Only when the process possesses sufficient ergodic properties can the scale parameter (v_c) of the empirical distribution of rupture slips be formulated according to the level of background noise (D), the driving force (F_{ext}) and the dissipation rate (F_C).

5.3 Implication to the concept of earthquake quanta

The representative Brownian particle for an earthquake in this study is very similar in concept to the seismon, which instantiates the seismic source as imaginary particles proposed by Wu et al. [81]. Wu et al. [81] defined an earthquake quantum as a basic elementary earthquake event composed of seismons, which are quasi-particles similar to the phonon in solid-state physics; accordingly, the statistical properties of an

481 earthquake phenomenon can be obtained through thermodynamic approaches. How-
 482 ever, in discussing the physical significance of the representative Brownian particle,
 483 we adopt a different interpretation from that of Wu et al. (1996). Wu et al. (1996)
 484 regarded the near-equilibrium problem of a “seismon gas” as a simplification of the
 485 earthquake source process at the timescale of only the occurrence of the mainshock.
 486 Thus, the scope of their model does not include the initiation/stopping mechanism,
 487 and shear slips are supposed to equally favor all directions. In this study, by regard-
 488 ing earthquake phenomena as transient frictional instabilities during the steady-state
 489 stochastic process of Coulomb friction, we simplify the problem of a tectonic process
 490 as a problem of Brownian particles in thermal equilibrium. The representative Brown-
 491 ian particle as the earthquake quantum allows statistical description of the mechanics
 492 of an infinitely extended slider-block system driven by an external constant force (F_{ext}
 493 in Eq. 1) with Coulomb friction damping (F_C in Eq. 1). The additional F_{ext} term
 494 as the driving force naturally causes the simulated rupture slips to prefer a specific
 495 direction, allowing a more realistic model for earthquake dynamics to be established.
 496 By instantiating earthquake activities as the sample paths of particles in the velocity
 497 space, we can generate a discussion in terms of an earthquake event and rupture slip.

498 6 Conclusion

499 In the conventional sense, an “earthquake event” denotes a local cluster of asperity
 500 failures that are able to be clearly distinguished on the human timescale. By regard-
 501 ing earthquakes as frictional instabilities in the collision of tectonic plates occurring
 502 steadily throughout the tectonic timescale, we propose to model the stochastic dynam-
 503 ics of earthquake ruptures by means of the Langevin equation and FPE. The proposed
 504 Langevin equation instantiates the earthquake rupture process as the sample path of
 505 the representative Brownian particle, with the diffusion term accounting for random
 506 collisions and chaotic interactions caused by the highly heterogeneous properties of
 507 fault planes. We obtain sample paths by numerically solving the Langevin equation and
 508 acquire the analytical distribution of the particle velocity by solving the correspond-
 509 ing FPE with the steady-state approximation. By regarding an event as a macroscopic
 510 slip session and considering local slips as the displacements in each microscopic step
 511 of the sample path, we can discuss the energy–duration relationship and the empiri-
 512 cal distribution of the rupture slips of earthquakes based on both the numerical and
 513 the analytical results. Regarding the slip distribution, we demonstrate that numeri-
 514 cally obtained samples generally follow the TEX model, which is obtained empirically
 515 based on the source model of large events worldwide. The FPE solution is generally
 516 a double-sided EXP function; however, for a process of finite duration with a large
 517 F_{ext}/F_C ratio that particularly favors the generation of large synthetic events, the FPE
 518 solution approximates the TEX model. This establishes the link between the physi-
 519 cal parameters in the Langevin equation and the scale parameter in the TEX model.
 520 Concerning the energy–duration relationship, a nearly constant scaling exponent of
 521 $n = 2/3$ for the power law $T \propto E_{\text{diss}}^n$ is observed among groups of events simulated
 522 with a broad range of physical parameters, suggesting a universal energy–duration
 523 scaling. Although the $T \propto E_{\text{diss}}^{2/3}$ proportionality obtained in this study is different

from the most common scaling of $T \propto M_0^{1/3}$ for general earthquake ruptures, the discrepancy may be attributed to the differences in the dimensionality of the model and the criteria for defining an event. However, it should be noted that the moment is not equivalent to energy, and the obtained $E_{\text{diss}} - T$ relationship depends solely on the numerically simulated results; further research must be conducted to discuss this topic in greater depth. Different versions of the Langevin equation have been adopted to investigate the dynamics of large many-body systems, for example, to predict the evolution of a vibrated granular system [82], to simulate the friction process at the nanoscale [83], and to establish a framework for earthquake dynamics [72, 84, 85]. With regard to earthquake dynamics, the Brownian walk model proposed by Ide (2008) for slow earthquakes and the traveling density wave model of Rundle et al. (1996) describe an earthquake rupture as a kind of stochastic process. Ide applied a typical Langevin equation with viscous damping to the rupture process of slow earthquakes by defining the overall rupture area as the random variable. For the traveling density wave model, in which a Langevin equation with a periodically changing force is applied to reproduce the quasi-periodical behavior of earthquake occurrence, Rundle et al. regarded an earthquake event as a sudden transition toward the minimal free energy of the fault system. Like these studies, this study successfully simplifies the highly complex problem of earthquake dynamics by means of Langevin's approach; thus, similar to the Brownian walk model and the traveling density wave model, our model is capable of producing scaling laws similar to empirically observed ruptures. As our model is idealized, several discrepancies between the physical meaning of our model and real scenarios should be noted. First, collisions or any other kinds of force interactions in a real seismogenic process have memory effects, but the interaction time in this study is assumed to be infinitesimal. Second, the simulated source processes in this study can differ considerably from a conventional earthquake. Whereas in a conventional earthquake rupture branches and develops asynchronously, our model limits rupture slip to take place consecutively one-by-one. Furthermore, as the proposed stochastic rupture process is always a Markov process, our model suggests sub-events that take places at different location on the same fault do not intercorrelate. Finally, the ruptures of real earthquakes evolve in two or more dimensions, while the Langevin equation discussed in this study is one dimensional. In the future, as this model is capable of reproducing source processes directly in the velocity space, additional insights into the scaling laws of seismology and statistical properties of earthquakes will be obtained. Moreover, the Langevin equation of Coulomb friction can be further generalized to fit more complex scenarios. For example, the Langevin equation can be dimensionally extended to simulate earthquake ruptures in two-dimensional space, and a periodical external force can be employed for seismic hazard assessments. Developments in probabilistic tsunami and seismic hazard assessments have also included the stochastic slip distributions of earthquakes to determine the overall probability distributions of particular tsunami heights or ground shaking levels [e.g., 86, 87]. Stochastic slip models quantify variations in slip to reasonably estimate the probability of a specified tsunami height or ground shaking intensity at an individual location resulting from a specific fault.

Acknowledgments. We would like to sincerely thank Prof. Jeen-Hwa Wang (Institute of Earth Sciences, Academia Sinica) for his substantial contribution to this work.

569 His insightful comments greatly improved the quality of our research, and we are grate-
570 ful for his valuable input and guidance throughout the revision of this manuscript. The
571 data underlying this article will be shared on reasonable request to the corresponding
572 author.

573 References

- 574 [1] Albertini, G., Karrer, S., Grigoriu, M.D., Kammer, D.S.: Stochastic properties
575 of static friction. *Journal of the Mechanics and Physics of Solids*, 104242 (2020)
576 <https://doi.org/10.1016/j.jmps.2020.104242>
- 577 [2] Brace, W.F., Byerlee, J.D.: Stick-Slip as a Mechanism for Earthquakes. *Science*
578 **153**(3739), 990–992 (1966) <https://doi.org/10.1126/science.153.3739.990>. Chap.
579 Reports
- 580 [3] Scholz, C.H.: The Mechanics of Earthquakes and Faulting. Cambridge University
581 Press, ??? (1990)
- 582 [4] Haessig, D.A., Friedland, B.: On the Modeling and Simulation of Friction. *Journal*
583 of Dynamic Systems, Measurement, and Control **113**(3), 354–362 (1991) <https://doi.org/10.1115/1.2896418>
- 584 [5] Kaproth, B.M., Marone, C.: Slow Earthquakes, Preseismic Velocity Changes, and
585 the Origin of Slow Frictional Stick-Slip. *Science* **341**(6151), 1229–1232 (2013)
586 <https://doi.org/10.1126/science.1239577>. Chap. Report
- 587 [6] Ruina, A.: Slip instability and state variable friction laws. *Journal of Geophysical*
588 Research: Solid Earth **88**(B12), 10359–10370 (1983) <https://doi.org/10.1029/JB088iB12p10359>
- 589 [7] Okubo, P.G., Dieterich, J.H.: Effects of physical fault properties on frictional
590 instabilities produced on simulated faults. *Journal of Geophysical Research: Solid*
591 *Earth* **89**(B7), 5817–5827 (1984) <https://doi.org/10.1029/JB089iB07p05817>
- 592 [8] Adjemian, F., Evesque, P.: Experimental study of stick-slip behaviour. *International*
593 *Journal for Numerical and Analytical Methods in Geomechanics* **28**(6),
594 501–530 (2004) <https://doi.org/10.1002/nag.350>
- 595 [9] Vargas, C.A., Basurto, E., Guzmán-Vargas, L., Angulo-Brown, F.: Sliding size
596 distribution in a simple spring-block system with asperities. *Physica A: Statistical*
597 *Mechanics and its Applications* **387**(13), 3137–3144 (2008) <https://doi.org/10.1016/j.physa.2008.01.108>
- 598 [10] Ohnaka, M., Kuwahara, Y., Yamamoto, K., Hirasawa, T.: Dynamic Break-
599 down Processes and the Generating Mechanism for High-Frequency Elastic
600 Radiation During Stick-Slip Instabilities. In: *Earthquake Source Mechanics*, pp.
601 13–24. American Geophysical Union (AGU), ??? (1986). <https://doi.org/10.1029/>

605 GM037p0013

- 606 [11] Moreno-Torres, L.R., Gomez-Vieyra, A., Lovallo, M., Ramírez-Rojas, A.,
607 Telesca, L.: Investigating the interaction between rough surfaces by using the
608 Fisher–Shannon method: Implications on interaction between tectonic plates.
609 *Physica A: Statistical Mechanics and its Applications* **506**, 560–565 (2018) <https://doi.org/10.1016/j.physa.2018.04.023>
- 610
- 611 [12] Wojewoda, J., Stefański, A., Wiercigroch, M., Kapitaniak, T.: Hysteretic effects
612 of dry friction: Modelling and experimental studies. *Philosophical Transactions of
613 the Royal Society A: Mathematical, Physical and Engineering Sciences* **366**(1866),
614 747–765 (2008) <https://doi.org/10.1098/rsta.2007.2125>
- 615
- 616 [13] Pei, L., Hyun, S., Molinari, J.F., Robbins, M.O.: Finite element modeling of
617 elasto-plastic contact between rough surfaces. *Journal of the Mechanics and
618 Physics of Solids* **53**(11), 2385–2409 (2005) <https://doi.org/10.1016/j.jmps.2005.06.008>
- 619
- 620 [14] Rivera, L., Kanamori, H.: Spatial heterogeneity of tectonic stress and friction in
621 the crust. *Geophysical Research Letters* **29**(6), 12–1124 (2002) <https://doi.org/10.1029/2001GL013803>
- 622
- 623 [15] Ohnaka, M., Akatsu, M., Mochizuki, H., Odedra, A., Tagashira, F., Yamamoto,
624 Y.: A constitutive law for the shear failure of rock under lithospheric conditions.
625 *Tectonophysics* **277**(1), 1–27 (1997) [https://doi.org/10.1016/S0040-1951\(97\)00075-9](https://doi.org/10.1016/S0040-1951(97)00075-9)
- 626
- 627 [16] Rundle, J.B., Turcotte, D.L., Shcherbakov, R., Klein, W., Sammis, C.: Statistical
628 physics approach to understanding the multiscale dynamics of earthquake
629 fault systems. *Reviews of Geophysics* **41**(4), 1019 (2003) <https://doi.org/10.1029/2003RG000135>
- 630
- 631 [17] Scholz, C.H., Aviles, C.A.: The Fractal Geometry of Faults and Faulting. In:
632 Earthquake Source Mechanics, pp. 147–155. American Geophysical Union (AGU),
633 ??? (1986). <https://doi.org/10.1029/GM037p0147>
- 634
- 635 [18] Carpinteri, A., Paggi, M.: A fractal interpretation of size-scale effects on strength,
friction and fracture energy of faults. *Chaos, Solitons and Fractals* **39**(2), 540–546
(2009)
- 636
- 637 [19] Goebel, T.H.W., Sammis, C.G., Becker, T.W., Dresen, G., Schorlemmer, D.: A
638 Comparison of Seismicity Characteristics and Fault Structure Between Stick-Slip
639 Experiments and Nature. *Pure and Applied Geophysics* **172**(8), 2247–2264 (2015)
<https://doi.org/10.1007/s00024-013-0713-7>
- 640
- 641 [20] Geller, R.J.: Scaling relations for earthquake source parameters and magnitudes.
Bulletin of the Seismological Society of America **66**(5), 1501–1523 (1976)

- 642 [21] Legrand, D.: Fractal Dimensions of Small, Intermediate, and Large Earthquakes.
643 Bulletin of the Seismological Society of America **92**(8), 3318–3320 (2002) <https://doi.org/10.1785/0120020025>
- 645 [22] Wang, J.-H.: A Review on Scaling of Earthquake Source Spectra. Surveys in
646 Geophysics **40**(2), 133–166 (2019) <https://doi.org/10.1007/s10712-019-09512-4>
- 647 [23] Brown, S.R., Scholz, C.H.: Closure of random elastic surfaces in contact. Journal
648 of Geophysical Research: Solid Earth **90**(B7), 5531–5545 (1985) <https://doi.org/10.1029/JB090iB07p05531>
- 650 [24] Brown, S.R., Scholz, C.H.: Broad bandwidth study of the topography of natural
651 rock surfaces. Journal of Geophysical Research: Solid Earth **90**(B14), 12575–
652 12582 (1985) <https://doi.org/10.1029/JB090iB14p12575>
- 653 [25] Renard, F., Candela, T.: Scaling of Fault Roughness and Implications for
654 Earthquake Mechanics. In: Fault Zone Dynamic Processes, pp. 195–215. Ameri-
655 can Geophysical Union (AGU), ??? (2017). Chap. 10. <https://doi.org/10.1002/9781119156895.ch10>
- 657 [26] Kagan, Y.Y.: Are earthquakes predictable? Geophysical Journal International
658 **131**(3), 505–525 (1997) <https://doi.org/10.1111/j.1365-246X.1997.tb06595.x>
- 659 [27] Aviles, C.A., Scholz, C.H., Boatwright, J.: Fractal analysis applied to character-
660 istic segments of the San Andreas Fault. Journal of Geophysical Research: Solid
661 Earth **92**(B1), 331–344 (1987) <https://doi.org/10.1029/JB092iB01p00331>
- 662 [28] Velde, B., Dubois, J., Moore, D., Touchard, G.: Fractal patterns of fractures
663 in granites. Earth and Planetary Science Letters **104**(1), 25–35 (1991) [https://doi.org/10.1016/0012-821X\(91\)90234-9](https://doi.org/10.1016/0012-821X(91)90234-9)
- 665 [29] Aki, K.: Magnitude-frequency relation for small earthquakes: A clue to the ori-
666 gin of f_{\max} of large earthquakes. Journal of Geophysical Research: Solid Earth
667 **92**(B2), 1349–1355 (1987) <https://doi.org/10.1029/JB092iB02p01349>
- 668 [30] Mai, P.M., Beroza, G.C.: A spatial random field model to characterize complexity
669 in earthquake slip. Journal of Geophysical Research: Solid Earth **107**(B11), 10–
670 11021 (2002) <https://doi.org/10.1029/2001JB000588>
- 671 [31] Lavallée, D., Liu, P., Archuleta, R.J.: Stochastic model of heterogeneity in
672 earthquake slip spatial distributions. Geophysical Journal International **165**(2),
673 622–640 (2006) <https://doi.org/10.1111/j.1365-246X.2006.02943.x>
- 674 [32] Sun, J., Yu, Y., Li, Y.: Stochastic finite-fault simulation of the 2017 Jiuzhaigou
675 earthquake in China. Earth, Planets and Space **70**(1), 128 (2018) <https://doi.org/10.1186/s40623-018-0897-2>

- 677 [33] Murphy, S., Herrero, A.: Surface rupture in stochastic slip models. *Geophysical Journal International* **221**(2), 1081–1089 (2020) <https://doi.org/10.1093/gji/ggaa055>
- 680 [34] Tsai, V.C., Hirth, G.: Elastic Impact Consequences for High-Frequency Earth-
681 quake Ground Motion. *Geophysical Research Letters* **47**(5), 2019–086302 (2020)
682 <https://doi.org/10.1029/2019GL086302>
- 683 [35] Einstein, A.: Investigation on the Theory of the Brownian Movement. Dover,
684 Mineola (2003)
- 685 [36] Renn, J.: Einstein's invention of Brownian motion. *Annalen der Physik* **14**(S1),
686 23–37 (2005) <https://doi.org/10.1002/andp.200410131>
- 687 [37] Hänggi, P., Marchesoni, F.: Introduction: 100years of Brownian motion. *Chaos: An Interdisciplinary Journal of Nonlinear Science* **15**(2), 026101 (2005) <https://doi.org/10.1063/1.1895505>
- 690 [38] Thingbaijam, K.K.S., Mai, P.M.: Evidence for Truncated Exponential Probability
691 Distribution of Earthquake Slip. *Bulletin of the Seismological Society of America*
692 **106** (4)(4), 1802–1816 (2016) <https://doi.org/10.1785/0120150291>
- 693 [39] Ohnaka, M.: A constitutive scaling law and a unified comprehension for frictional
694 slip failure, shear fracture of intact rock, and earthquake rupture. *Journal of Geophysical Research: Solid Earth* **108**(B2) (2003) <https://doi.org/10.1029/2000JB000123>
- 697 [40] Aki, K.: Characterization of barriers on an earthquake fault. *Journal of Geophysical Research: Solid Earth* **84**(B11), 6140–6148 (1979) <https://doi.org/10.1029/JB084iB11p06140>
- 700 [41] Aki, K.: Asperities, barriers, characteristic earthquakes and strong motion prediction. *Journal of Geophysical Research: Solid Earth* (1984) <https://doi.org/10.1029/JB089IB07P05867>
- 703 [42] Kanamori, H., Stewart, G.S.: Seismological aspects of the Guatemala Earthquake
704 of February 4, 1976. *Journal of Geophysical Research: Solid Earth* **83**(B7), 3427–
705 3434 (1978) <https://doi.org/10.1029/JB083iB07p03427>
- 706 [43] Papageorgiou, A.S., Aki, K.: A specific barrier model for the quantitative description
707 of inhomogeneous faulting and the prediction of strong ground motion. I. Description
708 of the model. *Bulletin of the Seismological Society of America* **73**(3),
709 693–722 (1983) <https://doi.org/10.1785/BSSA0730030693>
- 710 [44] Byerlee, J.D.: Frictional characteristics of granite under high confining pressure.
711 *Journal of Geophysical Research* (1896–1977) **72**(14), 3639–3648 (1967) <https://doi.org/10.1029/JZ072i014p03639>

- 713 [45] Costamagna, R., Renner, J., Bruhns, O.T.: Relationship between fracture and
 714 friction for brittle rocks. *Mechanics of Materials* **39**(4), 291–301 (2007) <https://doi.org/10.1016/j.mechmat.2006.06.001>
- 716 [46] Burridge, R., Knopoff, L.: Model and theoretical seismicity. *Bulletin of the
 717 Seismological Society of America* **57**(3), 341–371 (1967)
- 718 [47] Gross, S.J.: Traveling Wave and Rough Fault Earthquake Models: Illuminating
 719 the Relationship Between Slip Deficit and Event Frequency Statistics. In: Rundle, J.B., Turcotte, D.L., Klein, W. (eds.) *Geocomplexity and the Physics
 720 of Earthquakes*, pp. 73–82. American Geophysical Union, ??? (2000). <https://doi.org/10.1029/GM120p0073>
- 723 [48] de Wit, C.C., Olsson, H., Astrom, K.J., Lischinsky, P.: A new model for control of
 724 systems with friction. *IEEE Transactions on Automatic Control* **40**(3), 419–425
 725 (1995) <https://doi.org/10.1109/9.376053>
- 726 [49] Liang, J., Fillmore, S., Ma, O.: An extended bristle friction force model with
 727 experimental validation. *Mechanism and Machine Theory* **56**, 123–137 (2012)
 728 <https://doi.org/10.1016/j.mechmachtheory.2012.06.002>
- 729 [50] Saltiel, S., Bonner, B.P., Mittal, T., Delbridge, B., Ajo-Franklin, J.B.: Experimental
 730 evidence for dynamic friction on rock fractures from frequency-dependent
 731 nonlinear hysteresis and harmonic generation. *Journal of Geophysical Research: Solid Earth* **122**(7), 4982–4999 (2017) <https://doi.org/10.1002/2017JB014219>
- 733 [51] Labuz, J.F., Zang, A.: Mohr–Coulomb Failure Criterion. *Rock Mechanics and Rock Engineering* **45**(6), 975–979 (2012) <https://doi.org/10.1007/s00603-012-0281-7>
- 736 [52] Zang, A., Stephansson, O.: Rock Fracture Criteria. In: Zang, A., Stephansson,
 737 O. (eds.) *Stress Field of the Earth's Crust*, pp. 37–62. Springer Netherlands,
 738 Dordrecht (2010). https://doi.org/10.1007/978-1-4020-8444-7_3
- 739 [53] Eckmann, J.-P.: Roads to turbulence in dissipative dynamical systems. *Reviews
 740 of Modern Physics* **53**(4), 643–654 (1981) <https://doi.org/10.1103/RevModPhys.53.643>
- 742 [54] Huang, J., Turcotte, D.L.: Are earthquakes an example of deterministic chaos?
 743 *Geophysical Research Letters* **17**(3), 223–226 (1990) <https://doi.org/10.1029/GL017i003p00223>
- 745 [55] Huang, J., Turcotte, D.L.: Chaotic seismic faulting with a mass-spring model and
 746 velocity-weakening friction. *pure and applied geophysics* **138**(4), 569–589 (1992)
 747 <https://doi.org/10.1007/BF00876339>
- 748 [56] Kubo, R.: The fluctuation-dissipation theorem. *Reports on Progress in Physics*

- 749 **29**, 255–284 (1966) <https://doi.org/10.1088/0034-4885/29/1/306>
- 750 [57] Jazwinski, A.H.: Stochastic Processes and Filtering Theory. Academic Press, ???
751 (1970)
- 752 [58] Cyganowski, S., Kloeden, P., Ombach, J.: From Elementary Probability to
753 Stochastic Differential Equations with MAPLE®. Springer Science & Business
754 Media, ??? (2001)
- 755 [59] Kampen, N.G.: Stochastic Processes in Physics and Chemistry. North-Holland,
756 ??? (1981)
- 757 [60] Lemons, D.S., Gythiel, A.: Paul Langevin’s 1908 paper “On the Theory of Brow-
758 nian Motion” [“Sur la théorie du mouvement brownien,” C. R. Acad. Sci. (Paris)
759 146, 530–533 (1908)]. American Journal of Physics **65**(11), 1079–1081 (1997)
760 <https://doi.org/10.1119/1.18725>
- 761 [61] Coffey, W.T., Kalmykov, Y.P., Waldron, J.T.: The Langevin Equation: With
762 Applications In Physics, Chemistry And Electrical Engineering vol. 10. World
763 Scientific, ??? (1996)
- 764 [62] Zorzano, M.P., Mais, H., Vazquez, L.: Numerical solution of two dimensional
765 Fokker—Planck equations. Applied Mathematics and Computation **98**(2), 109–
766 117 (1999) [https://doi.org/10.1016/S0096-3003\(97\)10161-8](https://doi.org/10.1016/S0096-3003(97)10161-8)
- 767 [63] Kanamori, H., Anderson, D.L.: Theoretical basis of some empirical relations in
768 seismology. Bulletin of the Seismological Society of America **65**(5), 1073–1095
769 (1975)
- 770 [64] Aki, K.: Earthquake Mechanism. In: Ritsema, A.R. (ed.) Developments in Geo-
771 tectonics. The Upper Mantle, vol. 4, pp. 423–446. Elsevier, ??? (1972). <https://doi.org/10.1016/B978-0-444-41015-3.50029-X>
- 773 [65] Furumoto, M., Nakanishi, I.: Source times and scaling relations of large earth-
774 quakes. Journal of Geophysical Research: Solid Earth **88**(B3), 2191–2198 (1983)
775 <https://doi.org/10.1029/JB088iB03p02191>
- 776 [66] Tanioka, Y., Ruff, L.J.: Source Time Functions. Seismological Research Letters
777 **68**(3), 386–400 (1997) <https://doi.org/10.1785/gssrl.68.3.386>
- 778 [67] Houston, H.: Influence of depth, focal mechanism, and tectonic setting on the
779 shape and duration of earthquake source time functions. Journal of Geophysi-
780 cal Research: Solid Earth **106**(B6), 11137–11150 (2001) <https://doi.org/10.1029/2000JB900468>
- 782 [68] Michel, S., Gualandi, A., Avouac, J.-P.: Similar scaling laws for earthquakes and
783 Cascadia slow-slip events. Nature **574**(7779), 522–526 (2019) <https://doi.org/10.1038/s41586-019-1132-2>

- 785 [69] Ide, S., Beroza, G.C., Shelly, D.R., Uchide, T.: A scaling law for slow earthquakes.
786 Nature **447**(7140), 76–79 (2007) <https://doi.org/10.1038/nature05780>
- 787 [70] Aguiar, A.C., Melbourne, T.I., Scrivner, C.W.: Moment release rate of Casca-
788 dia tremor constrained by GPS. Journal of Geophysical Research: Solid Earth
789 **114**(B7) (2009) <https://doi.org/10.1029/2008JB005909>
- 790 [71] Gao, H., Schmidt, D.A., Weldon, R.J.: Scaling Relationships of Source Parameters
791 for Slow Slip EventsScaling Relationships of Source Parameters for Slow Slip
792 Events. Bulletin of the Seismological Society of America **102**(1), 352–360 (2012)
793 <https://doi.org/10.1785/0120110096>
- 794 [72] Ide, S.: A Brownian walk model for slow earthquakes. Geophysical Research
795 Letters **35**(17), 17301 (2008) <https://doi.org/10.1029/2008GL034821>
- 796 [73] Gomberg, J., Wech, A., Creager, K., Obara, K., Agnew, D.: Reconsidering earth-
797 quake scaling. Geophysical Research Letters **43**(12), 6243–6251 (2016) <https://doi.org/10.1002/2016GL069967>
- 799 [74] Scholz, C.H.: Scaling laws for large earthquakes: Consequences for physical
800 models. Bulletin of the Seismological Society of America **72**(1), 1–14 (1982)
- 801 [75] Ide, S., Imanishi, K., Yoshida, Y., Beroza, G.C., Shelly, D.R.: Bridging the
802 gap between seismically and geodetically detected slow earthquakes. Geophysical
803 Research Letters **35**(10) (2008) <https://doi.org/10.1029/2008GL034014>
- 804 [76] Frank, W.B., Rousset, B., Lasserre, C., Campillo, M.: Revealing the cluster of
805 slow transients behind a large slow slip event. Science Advances **4**(5), 0661 (2018)
806 <https://doi.org/10.1126/sciadv.aat0661>. Chap. Research Article
- 807 [77] Thøgersen, K., Sveinsson, H.A., Scheibert, J., Renard, F., Malthe-Sørenssen, A.:
808 The Moment Duration Scaling Relation for Slow Rupture Arises From Transient
809 Rupture Speeds. Geophysical Research Letters **46**(22), 12805–12814 (2019) <https://doi.org/10.1029/2019GL084436>
- 811 [78] Von Plato, J.: Boltzmann’s ergodic hypothesis. Archive for History of Exact
812 Sciences **42**(1), 71–89 (1991) <https://doi.org/10.1007/BF00384333>
- 813 [79] Gray, R.M.: Ergodic Theorems. In: Gray, R.M. (ed.) Probability, Random Pro-
814 cesses, and Ergodic Properties, pp. 239–262. Springer US, Boston, MA (2009).
815 https://doi.org/10.1007/978-1-4419-1090-5_8
- 816 [80] Pavliotis, G.A.: Stochastic Processes and Applications: Diffusion Processes, the
817 Fokker-Planck And Langevin Equations. Texts in Applied Mathematics. Springer-
818 Verlag, New York (2014). <https://doi.org/10.1007/978-1-4939-1323-7>

- 819 [81] Wu, Z.L., Chen, Y.T., Kim, S.G.: Physical significance of earthquake quanta.
820 Bulletin of the Seismological Society of America **86**(5), 1623–1626 (1996)
- 821 [82] Hayakawa, H.: Langevin equation with Coulomb friction. Physica D: Nonlinear
822 Phenomena **205**(1-4), 48–56 (2005) <https://doi.org/10.1016/j.physd.2004.12.011>
- 823 [83] Vanossi, A., Manini, N., Urbakh, M., Zapperi, S., Tosatti, E.: Modeling friction:
824 From nanoscale to mesoscale. Reviews of Modern Physics **85**(2), 529–552 (2013)
825 <https://doi.org/10.1103/RevModPhys.85.529> arXiv:1112.3234
- 826 [84] Rundle, J.B., Klein, W., Gross, S.: Dynamics of a traveling density wave model
827 for earthquakes. Physical Review Letters **76**(22), 4285–4288 (1996) <https://doi.org/10.1103/PhysRevLett.76.4285>
- 829 [85] Ide, S., Yabe, S.: Two-Dimensional Probabilistic Cell Automaton Model for
830 Broadband Slow Earthquakes. Pure and Applied Geophysics **176**(3), 1021–1036
831 (2019) <https://doi.org/10.1007/s00024-018-1976-9>
- 832 [86] Geist, E.L., Parsons, T.: Probabilistic Analysis of Tsunami Hazards*. Natural
833 Hazards **37**(3), 277–314 (2006) <https://doi.org/10.1007/s11069-005-4646-z>
- 834 [87] Geist, E.L., Parsons, T.: Assessment of source probabilities for potential tsunamis
835 affecting the U.S. Atlantic coast. Marine Geology **264**(1-2), 11 (2009) <https://doi.org/10.1016/j.margeo.2008.08.005>

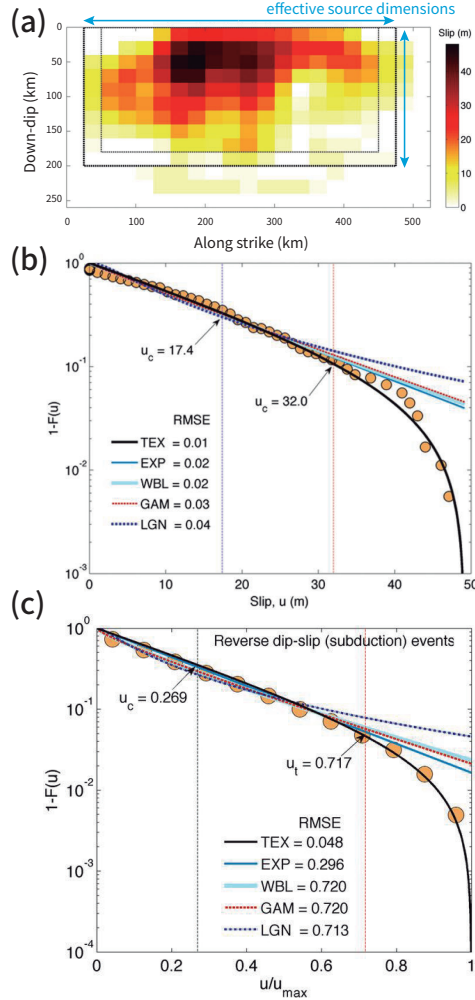


Fig. 3 The empirical TEX law for earthquake rupture slips proposed by Thingbaijam and Mai (2016). (a) [modified from Figure 1 (a) in Thingbaijam and Mai (2016)] The slip distribution from the finite source inversion for the 2011 Tohoku earthquake. (b) [Figure 1 (b) in Thingbaijam and Mai (2016)] The CCDF of the slip distribution of (a). In this subplot, orange circles denotes the empirical CCDF computed from the source model that is trimmed to the effective source dimensions; colored-solid or -dashed lines denotes the best fitting models of various distribution functions. (c) [the upper-left panel in the Figure 4 of Thingbaijam and Mai (2016)] The averaged CCDF of the slip distributions of subduction zone earthquakes worldwide. For the EXP and TEX distribution function, see Eq. 10 and Eq. 11 in this study; for the Weibull (WBL), Gamma (GAM) and lognormal (LGN) distributions, please refer to the Table 1 in the study of Thingbaijam and Mai (2016).

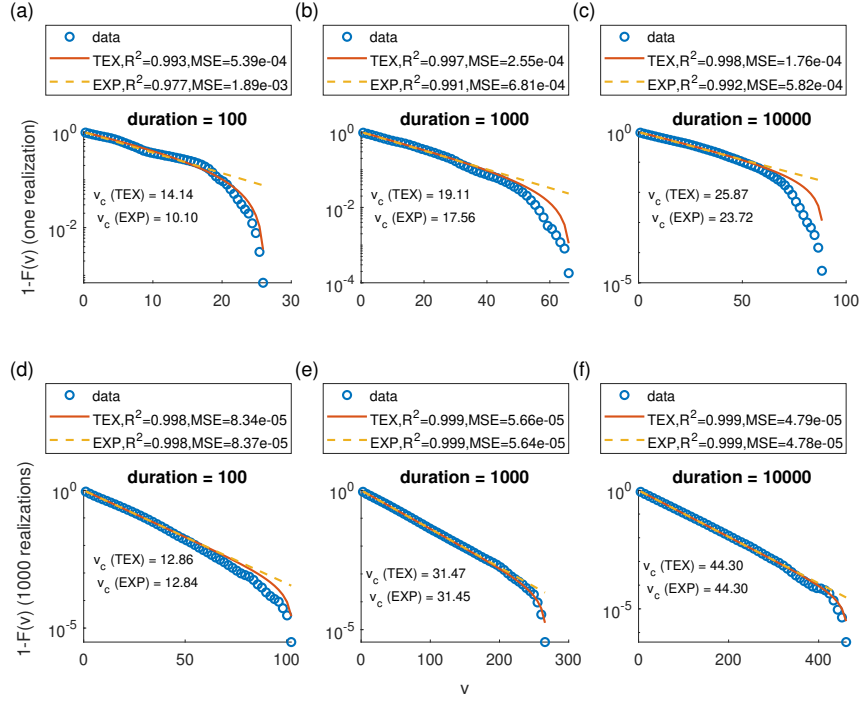


Fig. 4 The CCDF of synthetic slip velocities of different durations ($T = 10, 100$, and 1000), and their best fitting TEX and EXP model (red solid and orange dashed curve, respectively). The slip velocities are sampled evenly spaced in time from the particular solutions of Eq. 4, where $D = 5$, $F_C = 1$, $F_{\text{ext}} = 0.9$. In (a), (b), and (c), velocities for each distribution are collected from a single realization; in (d), (e), and (f), velocities for each distribution are collected from 1000 realization.

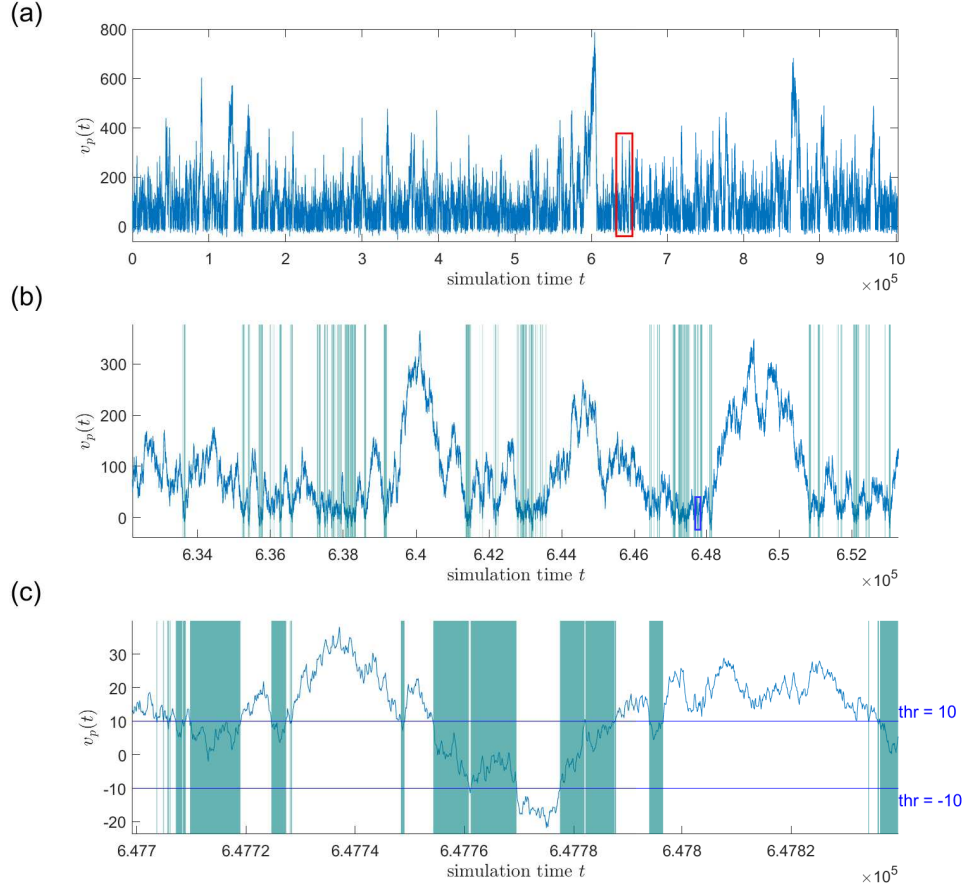


Fig. 5 The demonstration of how a sample path obtained from numerically solving the Langevin equation is subdivided into segments (namely, simulated events) in this study, with an exemplary threshold of detection $v_{\text{thr}} = 10$. (a) The entire sample path of $T \approx 10^6$ simulation time, with $D = 10$, $F_C = 1$, $F_{\text{ext}} = 0.9$. (b) Zoom up of (a) (red region in (a)). (c) Zoom up of (b) (blue rectangle in (b)). In subplots (b) and (c), the shaded area marks the intervals in which $|v_p(t)| \leq v_{\text{thr}}$ is satisfied, being the divisions between events.

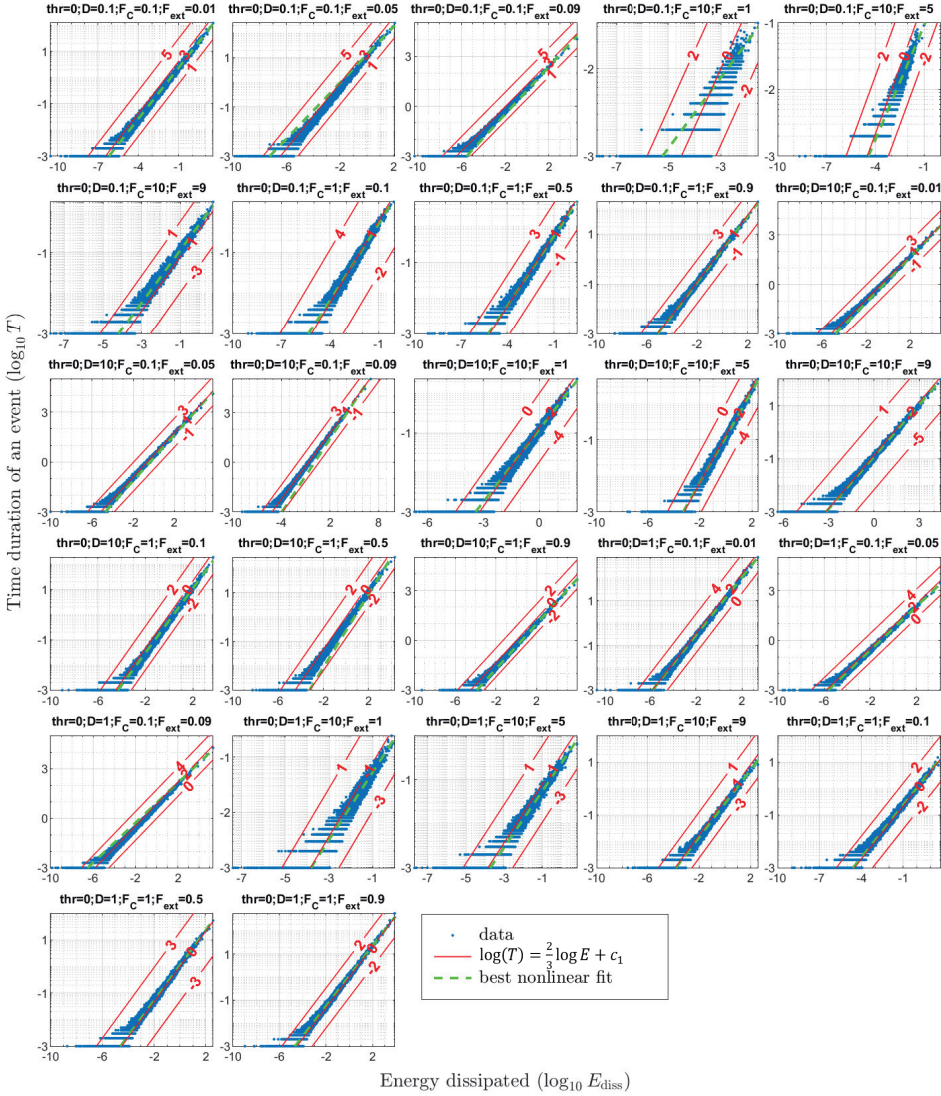


Fig. 6 The energies dissipated in and the durations of the simulated events generated by the Langevin equation of Coulomb friction (Eq. 1 and 4). The threshold defining an detectable event is $v_{\text{thr}} = 0$. The particular solutions are generated with $D = \{0.1, 1, 10\}$, $F_C = \{0.1, 1, 10\}$ and $F_{\text{ext}} = \{0.1F_C, 0.5F_C, 0.9F_C\}$. In each panel, the green dashed line is the best nonlinear fit to the data, with the fitting parameters of each fit (intercept c_1 and slope c_2 in log space) listed in Table 1; the red solid lines are the contour of $c_1 = \log T - (2/3) \log E$. The log without a subscript denotes the natural logarithm.

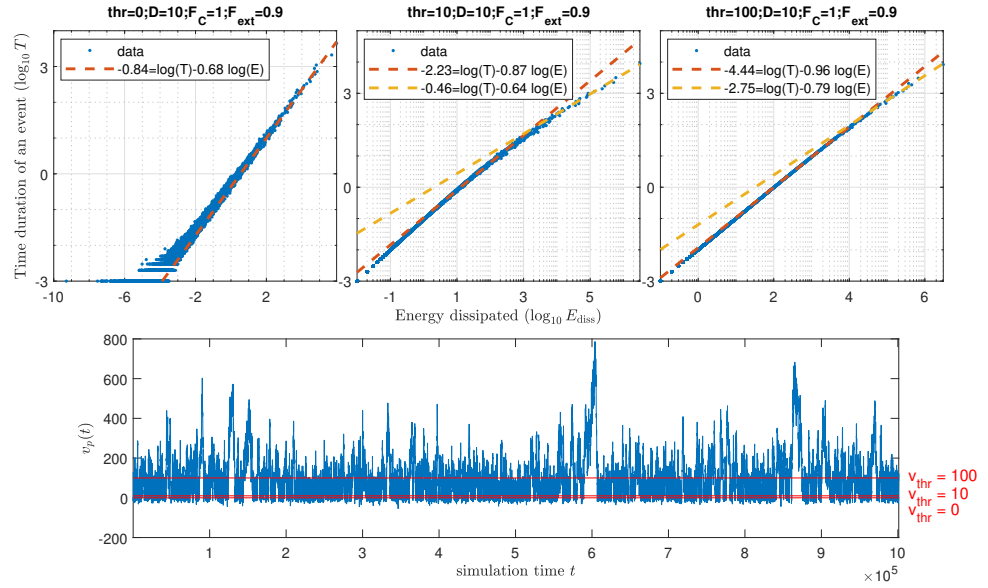


Fig. 7 The total energies dissipated v.s. the durations of simulated events defined by different thresholds (namely, $v_{\text{thr}} = 0, 10, 100$); the particular solution is generated with $D = 10$, $F_C = 1$, $F_{\text{ext}} = 0.9$. The log without a subscript denotes the natural logarithm.